Composites Part B 281 (2024) 111540

Contents lists available at ScienceDirect

Composites Part B

journal homepage: www.elsevier.com/locate/composites

Effect of low temperature on interlaminar fracture toughness of multi-directional CFRP and CFRP-steel interfaces

J. Koord [a,*], C. Hühne [b]

[a] German Aerospace Center (DLR), Institute of Lightweight Systems, Ottenbecker Damm 12, 21684 Stade, Germany
[b] German Aerospace Center (DLR), Institute of Lightweight Systems, Lilienthalplatz 7, 38108 Braunschweig, Germany

ARTICLE INFO

Keywords:
A. hybrid
B. fracture toughness
B. residual/internal stress
D. mechanical testing

ABSTRACT

Delamination is the dominant failure type in FMLs, particularly when combining CFRP and steel. Practical applications usually contain multi-directional interfaces. Therefore, delamination of multi-material and multi-directional interfaces is investigated using the DCB and ENF setups. Analysis of such interfaces requires asymmetric layups. Thus, thermal residual stresses (TRS) build up. Effects of TRS are corrected to compare true fracture toughness values, since neglecting TRS can result in mispredictions of up to 200 %. The ply orientation at the delamination interface affects the fracture toughness of monolithic and hybrid interfaces. In general, hybrid interfaces exhibit slightly lower interface properties compared to monolithic interfaces. While mode I behavior appears mostly unaffected by temperature, mode II fracture toughness slightly increases with decreasing temperature.

1. Introduction

CFRP is broadly used in lightweight design due to its high stiffness and strength at low density. However, CFRP also exhibits some drawbacks such as low bearing strength and a comparably low impact resistance in combination with a high risk of delamination. In contrast, metals show high bearing strength and good impact properties, but at the same time exhibit high density and poor fatigue resistance. By combining composites and metals, the drawbacks of each material group can be overcome. GLARE, combining aluminum and GFRP, is a well known example of a fiber metal laminate (FML) exhibiting excellent fatigue properties at a much lower weight than pure aluminum [1–3]. Other material combinations include for example the combination of CFRP and titanium, where good compatibility of material stiffness and coefficient of thermal expansion (CTE) lead to high strength and temperature resistance even under extreme temperature conditions [4,5], thus providing a high performance material e.g. for application as load-carrying shielding-structures in supersonic applications [6]. The high bearing strength makes CFRP-titanium FMLs also a good candidate for highly loaded mechanically fastened joints [7,8]. By combining CFRP and steel, a very high increase in stiffness and strength can be achieved at much lower metal contents compared to CFRP-titanium FMLs. Superior bearing capacity [8–10] as well as high impact resistance [11] is demonstrated. However, a drawback is the difficulty in machining because of high wear on toolings [12].

Nonetheless, as a result of the relatively large difference in many material properties, e.g. stiffness or CTE, some challenges still need to be overcome in order to fully exploit the advantages of steel hybridization in CFRP laminates. In addition to manufacturing challenges [13] and the determination of thermal residual stresses (TRS) [13,14], in particular the delamination behavior needs to be investigated as layer separation poses one of the dominating failure types in CFRP-steel FMLs [15,16].

The delamination behavior in terms of fracture toughness is described by the critical energy release rate (cERR). It is influenced by the quality of surface preparation of the metal surface as well as the magnitude of TRS at the interface under investigation [17]. Several test methods are proposed for investigating the cERR in composites. The double-cantilever-beam (DCB) test, standardized in ASTM D5528 [18], is used for termining the cERR under mode I loading, i.e. peel loads. The end-notched flexure (ENF) test, standardized in ASTM D7905 [19], can be applied for determining the cERR under mode II loading, i.e. shear loads. Further, tests to determine the cERR in mode III (transverse shear) or combinations of the modes (mode-mixity) are possible, too. From investigations on monolithic composites, it is known that crack propagation between adjacent layers of different orientation leads to different cERR values [16,20–23]. One reason is the different area of the resulting micromechanical fracture surface [24]. Studies on the behavior of multi-material interfaces as well as the effect of temperature are less prevailing.

* Corresponding author.
E-mail address: josef.koord@dlr.de (J. Koord).

https://doi.org/10.1016/j.compositesb.2024.111540
Received 3 December 2023; Received in revised form 23 March 2024; Accepted 7 May 2024
Available online 14 May 2024

Table 1
Specimen layups for interface testing in DCB and ENF setup.

Interface	Layup	D_c [–]	B_t [–]	l_{DCB} [mm]	l_{ENF} [mm]	b [mm]	t_{nom} [mm]
00//00	$[0_{17}//0_{17}]$	0.006	0.04	200	150	25	4.5
00//45	$[(0_2/90)_6, 0_2//45,(0_2/90)_6, 0_2]$	0.002	0.05	200	150	25	5.4
00//90	$[(0_2/90)_6, 0_2//90,(0_2/90)_6, 0_2]$	0.002	0.05	200	150	25	5.4
St//00	$[0_{16}$,St$//0_{17}]$	0.006	0.04	200	150	25	4.5
St//45	$[(0_2/90)_6$,0,St$//45,(0_2/90)_6, 0_2]$	0.002	0.05	200	150	25	5.4
St//90	$[(0_2/90)_6$,0,St$//90,(0_2/90)_6, 0_2]$	0.002	0.05	200	150	25	5.4

1.1. Multi-material interfaces

Within the scope of adhesive testing, the common configuration for hybrid interface analysis is characterized by the case where the adherents themselves are made of different materials [25–27]. However, it should be noticed that in the present research, multi-material interfaces are discussed with a focus on intrinsic FMLs (see Table 1) without any additional adhesive layer between metal and composite. Rather, the individual plies of the laminate are made from different materials. Both [10], Monden [17] and Petersen [9] investigate multi-material interfaces in CFRP-steel and CFRP-titanium FMLs. The manufacturing processes for the FMLs are similar, combining an abrasive metal pretreatment process (e.g. vacuum grit-blasting) followed by a chemical process (e.g. Sol–gel application) in order to ensure adhesion of the metal to the CFRP matrix system within a standard prepreg manufacturing process. All three studies agree on the fact that hybrid interfaces exhibit lower interlaminar fracture thoughness compared to monolithic interfaces at room temperature (RT). According to Petersen [9], microscopy of the interfaces after testing shows a combination of adhesive and cohesive failure at the interface since the metal surface is partially covered with resin and debris of fibers. Investigations by Both [10] on the evolution of the ERR in mode I with increasing crack length indicates that an R-curve effect is present only for hybrid interfaces (St//00, Ti//00) and not for the monolithic interface 00//00. An R-curve (resistance curve) behavior is defined by increasing fracture toughness with increasing crack length. Therein, fiber-bridging at the cracked interface and crack-jumping to adjacent interfaces resulting in multiple crack planes are determined as the source for the occurrence of an R-curve behavior. It should be noted, however, that Petersen [9] did not observe an R-curve effect in neither hybrid nor monolithic interfaces.

1.2. Multi-directional interfaces

Currently prevaling standards for mode I and mode II interlaminar testing, e.g. the DCB and ENF setups, are explicitly only valid for UD-0° laminates, and thus for 00//00 interfaces. However, in practical applications multi-directional laminate layups are present and delamination is usually observed between layers of different orientations [28]. Thus, it is important to study multi-directional interfaces.

By nature, testing of multi-directional – and for that matter multi-material interfaces – requires asymmetric layups with respect to the fracture plane. Thus, the bending-twisting coupling terms in the stiffness matrix of the laminate become non-zero. As a result, parasitic effects leading to non-perfect mode isolation are present and should be taken into account. Different authors investigate multi-directional interfaces in monolithic composites, coming to conflicting findings: Pereira et al. [20] and Chai [29] observe that both mode I and mode II interlaminar fracture toughness are independant of the orientation of the plies at the interface under investigation. However, Tao and Sun [30] as well as Bienas [31] report that the interlaminar fracture toughness decreases as the difference in ply-angle between adjacent layers increases.

When considering multi-directional interfaces in FMLs, result are rare. Petersen [9] investigates CFRP-St FMLs at RT with interfaces including St//00, St//45 and St//90 in the DCB as well as ENF test setup. The fracture toughness of the St//00 interface in mode I is lower compared to St//45 and St//90 interfaces. However, the mode II fracture toughness of the St//00 interface is larger compared to St//45 and St//90 interfaces. Similar results are reported by Bienias et al. [31] for GFRP-aluminum and CFRP-aluminum FMLs for the ENF case. For both material combinations the interfaces composed of metal and 0° layers exhibit the highest mode II fracture toughness followed by metal//45 and metal//90 interfaces. Except for Petersen [9], who improves the layup of the specimens to reduce parasitic effects resulting from asymmetry, neither of the remaining studies quantify the effect of parasitic modes affecting the characterization of delamination behavior.

1.3. Effect of low temperature

The common assumption regarding delamination at low temperature conditions is that the matrix strength increases with decreasing temperature, and thus the delamination resistance is considered to increase, too. However, results from literature report conflicting observations regarding the effect of low temperature on delamination in composites: Asp [32] investigates the low temperature behavior of monolithic CFRP specimens in the DCB and ENF configuration at RT and −50 °C. Despite testing asymmetric specimen layups, effects of parasitic mode interaction and TRS on the cERR are not taken into account. Within the study, the apparent fracture toughness in mode I is not affected, whereas the fracture toughness in mode II increases significantly with decreasing temperature. A study by Kim et al. [33] on DCB specimens at temperatures as low as −100 °C shows that the fracture toughness in mode I increases with decreasing temperature. According to Coronado et al. [34–36], the mode I cERR for temperatures down to −60 °C decreases with decreasing temperature.

Only very limited literature can be found on the effect of low temperature on delamination in CFRP-steel interfaces in terms of fracture toughness analysis. Rather, most research on FMLs regarding this topic focuses on GLARE by investigating the fatigue crack growth behavior. In that regard, studies suggest that lower temperatures reduce the crack growth rates in GLARE [37–39]. An investigation by Burianek [40] on delamination in CFRP-titanium face sheets at −18 °C indicates increasing delamination resistance with decreasing temperature. Similar observations are made by Rans et al. [41] on the delamination growth rates for GLARE as well as CFRP-titanium FMLs at −40 °C.

The investigation of multi-material and multi-directional interfaces results in testing of asymmetric specimens, which is why inclusion of parasitic effects due to layup and TRS on the derivation of the fracture toughness value from the experiment is important [17,42,43]. The necessity for accounting for parasitic effects during data reduction is demonstrated in Koord et al. [44]. Especially in case of CFRP-steel FMLs, large errors in delamination prediction can occur if data reduction is not done appropriately. Within the study, a comprehensive correction methodology is described and validated extensively. This methodology for retrieving true fracture toughness values from experimental testing is also applied in the present study.

In the present research, the effect of temperature on the delamination behavior of multi-material and multi-directional interfaces is investigated. For this purpose, mode I and mode II delamination analysis based on DCB and ENF testing is conducted at RT (23 °C) and LT (−55 °C). Thereby, the goal is to contribute to closing the gap

in literature regarding the delamination behavior of CFRP-steel FMLs, explicitly regarding the effects of temperature and multi-directional interfaces. Monolithic interfaces are investigated as well in order to provide a reference for the discussion on the effects of temperature and multi-directional interfaces.

2. Experimental work

In the present section, an overview on the methodology for determining true ERR values as well as a description of the manufacturing, testing, and data reduction process is given.

2.1. Determination of true fracture toughness

Investigation of the interlaminar behavior is based on the DCB and ENF test setups for mode I and mode II characterization, respectively. These methods have been proven to be applicable to monolithic as well as hybrid interfaces [9,10,17]. The determination of interface properties is sensitive to non-uniform behavior. Therefore, the apparent energy release rate (aERR) resulting directly from the experiment needs to be corrected in order to yield the true energy release rate (tERR) [45]. Monolithic specimens are affected by non-uniformities just as hybrid specimens are. However, in case of hybrid specimens parasitic effects are usually more pronounced.

Since the sources of these parasitic effects are manifold, different correction types are distinguished in Fig. 1. While measures like the sublaminate technique to minimize effects due to asymmetric layups are introduced during specimen manufacturing, correction for large deformations, load introduction and beam compliance are conducted during evaluation of the test results. In turn, correcting effects arising from thermal residual stresses is usually done by applying correction terms on the energy release rate after evaluation of the test results. Application of the individual steps for determining the tERR are introduced and discussed individually in the subsequent sections. Validation of the methodology for CFRP-steel FMLs is provided in Koord et al. [44].

2.2. Specimen manufacturing

Specimen manufacturing is done using CFRP prepreg material by Hexcel (HexPly M21/35%/134 gsm/T700GC) with a cured ply thickness of 0.13 mm. For the FML specimens, austenitic steel 1.4310 with a nominal foil thickness of 0.13 mm is used. Prior to layup, the metal sheets undergo a pre-treatment process in order to assure accurate bonding to the CFRP layers. The process developed at DLR combines mechanical and chemical treatment by vacuum grit-blasting and Sol–gel application [50]. Grit-blasting is conducted with an abrasive media (KB105) at a feed rate of 0.5 mm/s. The steel foil is then immersed in Sol–gel (AC-130-2) for 150 s and dried for 60 min before being covered with prepreg material. A total of six plates are manufactured by hand layup, vacuum sealed, and cured in an autoclave following the manufacturer's recommended curing cycle. The initial pre-crack in the midplane of the laminates is introduced by insertion of a double-layered PTFE foil of 25 μm in thickness. After curing, the specimens are cut out of the plates by waterjet and measured using a micrometer. The DCB specimens are further processed by applying piano hinges at the ends of the free specimen sublaminates for the load introduction conforming to ASTM D5528. After manufacturing, the specimens are stored at 23 ± 3 °C and 50 ± 10% relative humidity until testing.

Testing of multi-directional and/or multi-material interfaces requires the laminate layup to be asymmetric by nature. However, in an attempt to minimize parasitic effects resulting from an asymmetric layup, recommendations for multi-directional interfaces [51] are adopted to the layups presented in Table 1. These layups have been previously validated for analysis of multi-directional and multi-material interfaces at RT by Petersen [9]. Adjusting the stacking sequence constitutes a correction for *effects arising from deviation from the beam theory* in Fig. 1. By adjusting the layup, a relatively even and symmetrical ERR profile across the specimen width is achieved through minimizing the curvature due to longitudinal/transverse-bending coupling as well as the skewness of the crack profile due to bending-twisting coupling of the specimen arms. Following conditions are defined by Prombut et al. [51] based on the laminate ABD-matrix $D_c \leq 0.25$ and $B_t \ll 1$, respectively:

$$D_c = \frac{D_{12}^2}{D_{11} D_{22}} \leq 0.25; \quad B_t = \left| \frac{D_{16}}{D_{11}} \right| \ll 1 \tag{1}$$

The layups shown in Table 1 have been previously validated for analysis of multi-directional and multi-material interfaces at RT by Petersen [9].

2.3. Test setup and procedure

Testing is conducted on two temperature levels, 23 °C and −55 °C, inside a temperature chamber in a servo-mechanic testing machine by Zwick (Zwick 1484) equipped with a 20 kN load cell. The temperature in the chamber is continuously monitored using two resistance temperature detectors (Pt100). In case of low temperature tests, the specimens are cooled inside the temperature chamber for 10 min prior to testing.

The DCB test setup in Fig. 2(a) is extended by a fullframe camera with a resolution of 42 mega pixel and a spotlight to assure consistent lighting conditions. Images are taken at a frequency of 1 Hz and synchronized with force, displacement, and temperature data. The setup was previously applied successfully at DLR [52,53]. Prior to testing, a natural pre-crack is introduced into the DCB specimen in order to prevent measurement of wrongfully high fracture toughness values. Pereira et al. [20] identified resin nests at the tip of the PTFE foil to lead to a significant error in determination of the cERR at crack initiation. Therefore, after placing the DCB specimen inside the testing rig, the crossbeam is slowly moved until the initial pre-crack length of 40 mm introduced by the PTFE foil is extended to $a_o = 43$ mm. Thereby, natural crack front develops, as is recommend for multi-directional interfaces. The actual test is conducted at a constant crosshead speed of 1 mm/min.

The ENF test is conducted in a three-point bend setup in Fig. 2(b). Monitoring of the crack front is not conducted because mode II testing in the present case is generally associated with instable crack propagation [54]. Inside the fixture, the ENF specimens are supported by two bottom legs at a distance of 100 mm while load introduction occurs by a center stamp at a constant crosshead speed of 0.5 mm/min. Different to the DCB setup, ENF specimens require manual alignment in order to assure that the initial crack length, defined by the distance between the support leg and the crack tip, is set accurately.

2.4. Experimental data reduction procedure

Determination of the interlaminar properties is based on the approaches offered in the standards for the DCB and ENF test, respectively. For DCB analysis, the compliance calibration (CC) method for data reduction is selected based on the recommendation by Yokozeki et al. [45] for inclusion of TRS in the analysis process. The CC method uses a least squares plot of $\log(\delta/P)$ over $\log(a)$. Therein, the slope of the linear least squares fit represents the correction factor n. The aERR based on the CC approach reads:

$$G_{Ic}^{exp} = \frac{nP\delta}{2ba} \tag{2}$$

Comparison of force–displacement data with the visual inspection of the crack propagation behavior indicates that the cERR at crack initiation G_{Ic} can be obtained from the maximum force during the experiment P_{max}.

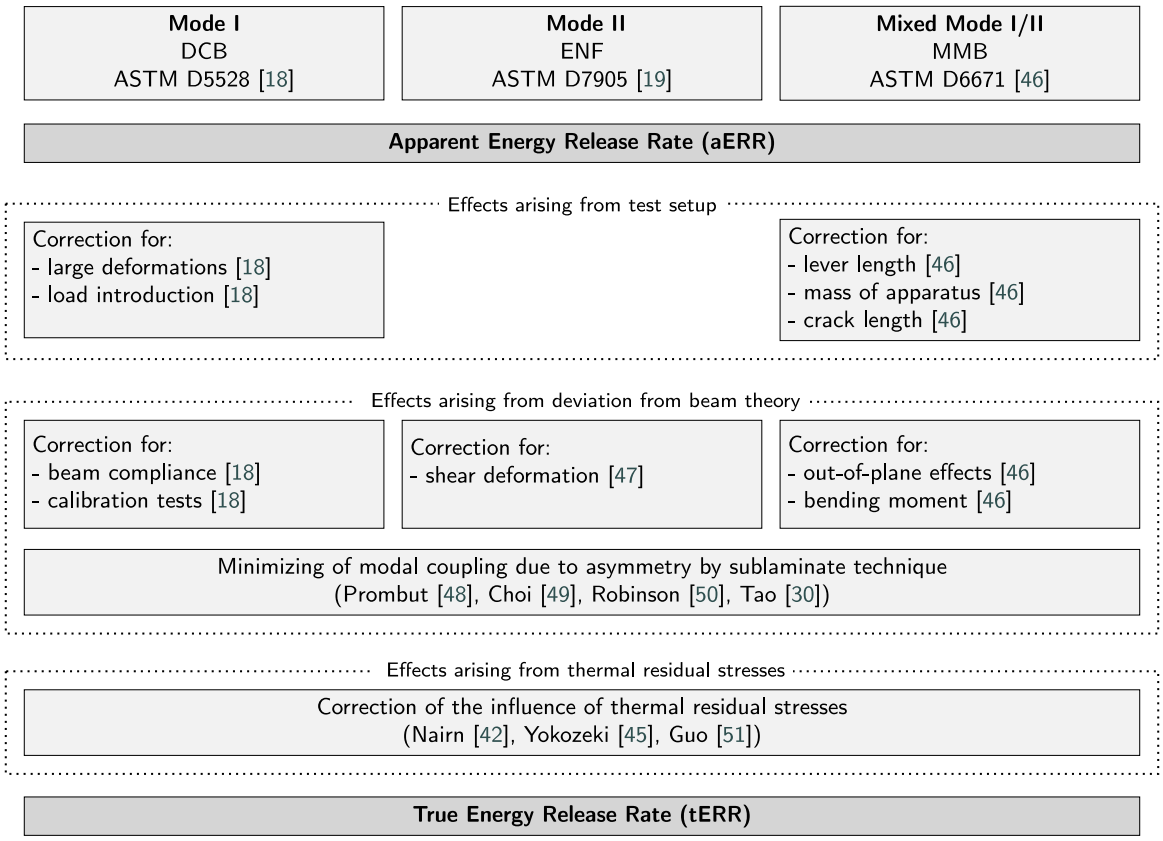

Fig. 1. Overview on methodology for determination of the true energy release rate by correction of apparent energy release rates influenced by the test setup, deviations from the beam theory, and TRS [44] (see [46–49]).

(a) Double-Cantilever-Beam (DCB) (b) End-Notched-Flexure (ENF)

Fig. 2. Test setup inside a thermal chamber for (a) DCB testing including camera setup and (b) ENF testing.

The CC method is adopted from ASTM D7905 for determining the cERR from the experimental ENF test data. One specimen out of each series is used to determine the compliance coefficient and loaded up to 50% of the maximum force from the fracture test whilst varying the crack length a_o from 15 mm to 25 mm to 35 mm. These compliances $(\delta/P)_{a_o}$ are then plotted over the crack length cubed a^3. The CC coefficients are obtained from a linear least squares regression analysis ($\delta/P = A + ma^3$), with A representing the intersect and m the slope of the regression function. The cERR in mode II results to:

$$G_{IIc}^{exp} = \frac{3mP_{max}^2 a_o^2}{2b} \tag{3}$$

As the data reduction methods in ASTM D5528 and ASTM D7905 are developed for monolithic specimens, it is assumed that the delamination modes are perfectly isolated during the DCB test (mode I) and the ENF test (mode II). However, in hybrid specimens mode-isolation is flawed. A detailed analysis on the degree of mode-isolation, i.e. the contribution of parasitic modes, is provided in Koord et al. [44]. The study on CFRP-steel interfaces shows that mode isolation is quite acceptable. Therein, the contribution of parasitic modes is less than 5% over the vast majority of the crack-tip length. Only at the edges of the specimens, parasitic modes become more prevailing and contribute to up to approximately 20% (DCB) and 35% (ENF) to the overall

Table 2
Apparent ERR of monolithic and hybrid interfaces in mode I (G_{Ic}^{exp}) and mode II (G_{IIc}^{exp}).

			G_{Ic}^{exp}						G_{IIc}^{exp}					
			00//00	00//45	00//90	St//00	St//45	St//90	00//00	00//45	00//90	St//00	St//45	St//90
23 °C (RT)	Mean	N/mm	0.311	0.384	0.598	0.374	0.551	0.371	2.402	2.916	2.226	1.707	1.897	2.114
	Std. Dev.	N/mm	0.017	0.029	0.067	0.044	0.039	0.013	0.094	0.090	0.115	0.197	0.136	0.075
	C.o.V.	%	5.50	7.48	11.2	11.7	6.99	3.63	6.93	3.08	5.18	11.5	7.16	3.56
	n	–	4	4	4	6	5	5	3	3	3	4	5	5
−55 °C (LT)	Mean	N/mm	0.322	0.387	0.585	0.400	0.524	0.436	2.506	3.022	2.182	1.808	2.049	1.806
	Std. Dev.	N/mm	0.034	0.038	0.060	0.029	0.024	0.039	0.133	0.291	0.118	0.264	0.088	0.126
	C.o.V.	%	10.2	9.83	10.2	7.27	4.54	9.01	5.30	9.62	5.39	14.6	7.97	6.96
	n	–	6	6	6	4	5	5	6	6	6	4	5	5

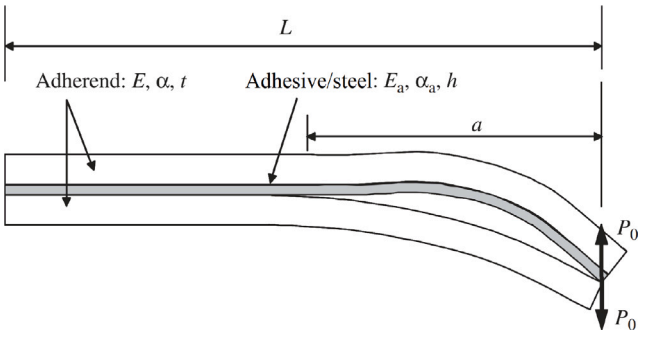

Fig. 3. Schematic representation of specimen tip loads as a result of a mismatch in CTE in asymmetric DCB specimen [55].

fracture energy G_{tot}. Regarding the effects on the global behavior of the force–displacement curve, these effects are negligible, which is why the methods from the standards are considered to be applicable to the present case. In Table 2, the aERR for the DCB and ENF tests determined by the CC method are summarized.

2.5. Correction of fracture toughness values

As previously discussed, the specimens in the present research contain multi-directional and multi-material interfaces, resulting in asymmetric layups (see Table 1). Hence, the thermal expansion behavior of the sublaminates differs. When subjected to a large temperature difference, TRS build up due to the differences in thermal shrinkage of the sublaminates. As a result, thermal loads are acting on the crack tip eventhough no external load is applied [42]. When considering the DCB specimen, the presence of TRS can lead to either a closing or an opening moment acting on the crack tip depending on the material properties and laminate layup at hand. Further, depending on the degree of asymmetry and the temperature difference ΔT, the magnitude of TRS differs, too. Inclusion of thermal effects is particularly important when dealing with CFRP-steel laminates, since the large difference in CTE combined with high stiffnesses of the constituents lead to a high level of TRS [44]. Testing at low temperatures further increases the residual stress state. These effects are currently not considered in the standards but should be incorporated when evaluating interlaminar properties of specimens with disimilar sublaminates. The present correction method represents the correction for *effects arising from thermal residual stresses* in Fig. 1.

In Yokozeki et al. [45], an analytical correction method for thermal effects in DCB and ENF specimens based on the formulations of Nairn [42] is presented. Therein, by dividing the specimen into three sublaminates, namely two cracked arms and the intact portion of the laminate, the aERR obtained from the experiment $G_{Ic/IIc}^{exp}$ is corrected by superimposing the fraction of ERR due to thermal effects $G_{I/II}^{th}$, thus, yielding the tERR.

It is important to note that the correction method by Yokozeki et al. [45] assumes no contact between the cracked arms of the specimen. This simplification is viable for most specimens. However, especially when considering asymmetric CFRP-steel FMLs contact forces need to be considered as demonstrated in detail in Koord et al. [44]. As shown at the example of a DCB specimen for characterization of an adhesive in Fig. 3, the mismatch in CTE between adhesive and adherend results in tensile TRS in the adhesive after cooling the specimen from the stress-free temperature during curing down to room temperature or low temperature levels. The two debonded arms touch each other at the tips, which in turn leads to contact forces. (The idea of a stress-free temperature was first introduced by Pagano and Hahn [56]. It assumes that during manufacturing the matrix in a composite is sufficiently viscoelastic above a certain temperature so that any stresses can relax. When cooling a composite down from the stress-free temperature an increase in TRS can be expected. The magnitude of TRS depends on the difference in CTE and stiffness of the constituents of a laminate. In case of a UD-0° specimen, there are no TRS present on meso-scale. In case of a hybrid laminate, the difference in CTE between metal and CFRP in combination with an asymmetric layup leads to the build-up of TRS, resulting in a curved specimen as can be seen in Fig. 3.) Guo et al. [55] have introduced a correction method to account for the additional deformation within the debonded region due to the existence of contact forces. In Koord et al. [44], it has further been demonstrated that by replacing the properties of the adhesive layer with properties of steel, the correction method can be transferred to hybrid laminates, since the difference in CTE between CFRP and adhesive ($CTE_{UD\text{-}0°} < CTE_{adhesive}$) is qualitatively similar to the difference in CTE between CFRP and steel ($CTE_{UD\text{-}0°} < CTE_{steel}$). The deformation shape is similar but more pronounced in case of the steel ply due to the larger stiffness of steel. Thus, the total ERR is obtained by superposition of the strain energies, which is why the portion of ERR at the crack tip $G_{I,tip}$ determined based on Guo et al. [55] is added onto the ERR correction terms by Yokozeki et al. [45]:

$$G_{Ic} = G_{Ic}^{exp} + \underbrace{\frac{P_{max}\Delta T}{b}(\alpha_{\kappa}^{(1)} - \alpha_{\kappa}^{(2)})a + \frac{\Delta T^2}{2b}(I^{(1)} + I^{(2)} - I^{(3)}) + G_{I,tip}^{th}}_{G_I^{th}} \tag{4}$$

$$G_{IIc} = G_{IIc}^{exp} + \underbrace{\frac{P_{max}\Delta T}{b}(\alpha_{\kappa}^{(2)} - \alpha_{\kappa}^{(3)})a + \frac{\Delta T^2}{2b}(I^{(1)} + I^{(2)} - I^{(3)})}_{G_{II}^{th}} \tag{5}$$

In Table 3, the correction thermals for mode I and mode II ERR are summarized. A brief derivation of the equations is presented in Appendices C.1 and C.2. For details on the correction methods for the cases with and without tip contact, the reader is referred to [45,55], respectively. While the correction method excluding tip forces has been applied repeatedly on adhesive joints with dissimilar adherents [57,58] as well as CFRP-steel FMLs [9,10,17], the consideration of tip forces is new for asymmetric CFRP-steel laminates.

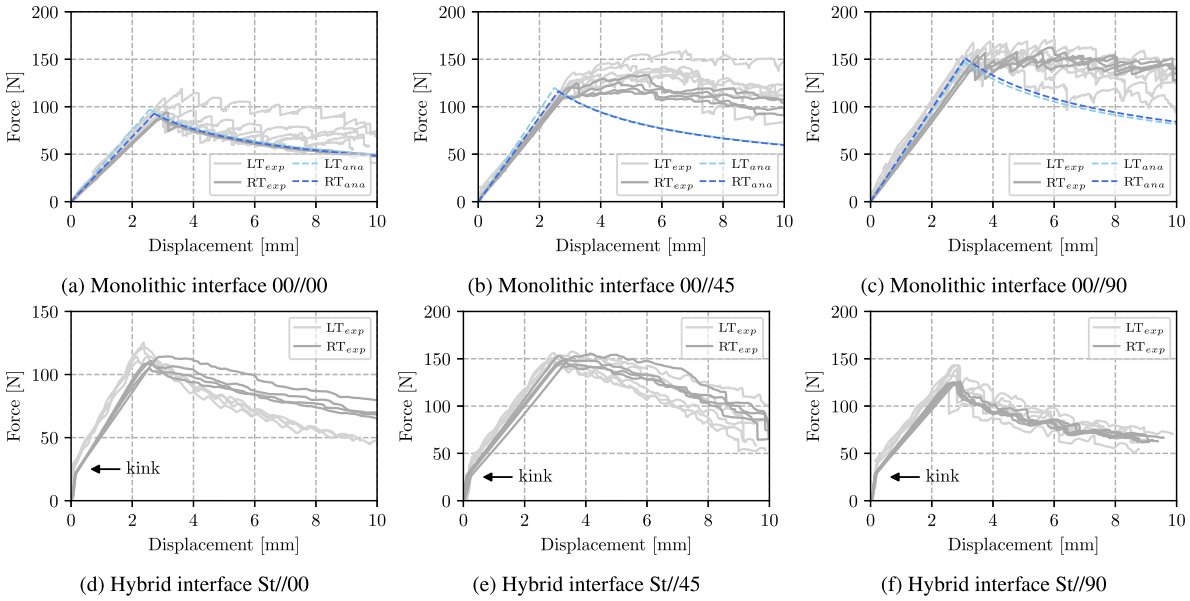

(a) Monolithic interface 00//00 (b) Monolithic interface 00//45 (c) Monolithic interface 00//90

(d) Hybrid interface St//00 (e) Hybrid interface St//45 (f) Hybrid interface St//90

Fig. 4. Force–displacement curves of DCB tests at 23 °C (RT) and −55 °C (LT).

Table 3
Correction terms for ERR in mode I and mode II due to thermal residual stresses $G^{th}_{I/II}$ in N/mm.

	Temp.	00//00	00//45	00//90	St//00	St//45	St//90
G^{th}_{I}	LT	0	−0.029	−0.023	−0.092	−0.141	−0.115
	RT	0	−0.019	−0.013	−0.048	−0.086	−0.060
G^{th}_{II}	LT	0	0.208	0.108	0.545	0.586	0.575
	RT	0	0.104	0.063	0.275	0.304	0.319

3. Results and discussion

3.1. Interlaminar behavior in mode I

The discussion of the DCB results is divided into four parts. First, the behavior of monolithic and hybrid specimens based on force–displacement data is studied. Then, the cERR defining delamination initiation and the importance of considering thermal effects are discussed, followed by an investigation on the evolution of ERR with increasing crack length. Finally, the fracture surfaces are compared.

3.1.1. Force–displacement curves

In Fig. 4, the force–displacement curves of the DCB tests are presented. In case of the monolithic specimens, analytically determined force–displacement curves based on Eq. (6) are calculated with temperature-dependent material properties and true ERR for verification. In case of the hybrid specimens, the kink in the curve behavior associated with the contact force at the tip of the cracked sublaminates does not allow for analytical verification.

In the monolithic laminates, the effects of TRS due asymmetry in the specimen layup are very small (see Fig. 5(a)). Therefore, verification by comparison to the analytically predicted curve behavior can be done with acceptable accuracy. However, in the hybrid laminates the assumption of the sublaminates having identical mechanical properties in Eq. (6) is violated. The sublaminate which contains the metal ply exhibits a curvature due to the bending moments that are introduced by the asymmetry (see Fig. 3). As a result, at the very beginning of the DCB test first the curvature is eliminated by the load increase at almost no displacement. Then, at the position of the kink, the sublaminates start to separate from one another. As this behavior is rooted in the presence of TRS, the kink in the load–displacement curves of specimens tested at LT are on a higher load level than for those tested at RT because the difference to the stress-free temperature is greater. For specimens that are tested at the stress-free temperature, theoretically, the kink would vanish. The present characteristic demonstrates the necessity of including thermal effects, in particular when studying hybrid specimens. A detailed investigation of this phenomenon is presented in Koord et al. [44].

In case of the 00//00, St//00 and St//90 interfaces, self-similar crack propagation after crack onset is observed. For the remaining interfaces, however, an R-curve effect is expected for the interfaces 00//45, 00//90 and to a smaller extent even in case of St//45.

3.1.2. Critical energy release rates

Fig. 5 shows the cERR in mode I for monolithic and hybrid interfaces at RT and LT. Based on the correction methodology in Fig. 1, the comparison in Fig. 5 differentiates between the aERR based on the experimental test G^{exp}_{Ic}, the thermal portion due to the asymmetric layup G^{th}_{I} as well as the tERR G_{Ic}.

Considering the monolithic interfaces in Fig. 5(a), correction of thermal effects is considered negligible because the correction terms are either smaller or on the same order of magnitude as the standard deviation during testing. However, when looking at the hybrid interfaces in Fig. 5(b), neglecting thermal effects leads to a significant overestimation of the cERR. Therefore, TRS need to be taken into account. Otherwise, comparison of hybrid interfaces is not accurate. Furthermore, delamination onset might be overestimated when using the aERR as input in numerical simulations in conjunction with cohesive element modeling.

Comparing the tERR at crack initiation G_{Ic}, the hybrid interfaces St//00 and St//45 exhibit comparable interfacial toughness when considering their monolithic counterparts at both RT and LT. The interface St//90 exhibits a lower fracture toughness than the interface 00//90. Similar behavior between monolithic and hybrid interfaces has been reported by Petersen [9] at RT. As can be seen in Fig. 7, crack onset in both the St//90 and 00//90 interfaces is affected by crack jumping, which highly influences the fracture toughness value. The 00//90 interface additionally shows fiber bridging, which could explain the difference in fracture toughness compared to the St//90 specimen.

Regarding the effect of low temperature on the fracture toughness, the monolithic interfaces appear to be not affected. This behavior is somewhat unexpected as the common assumption is that the true interface toughness, especially in monolithic CFRP, increases with decreasing temperature as the matrix properties improve. In comparison

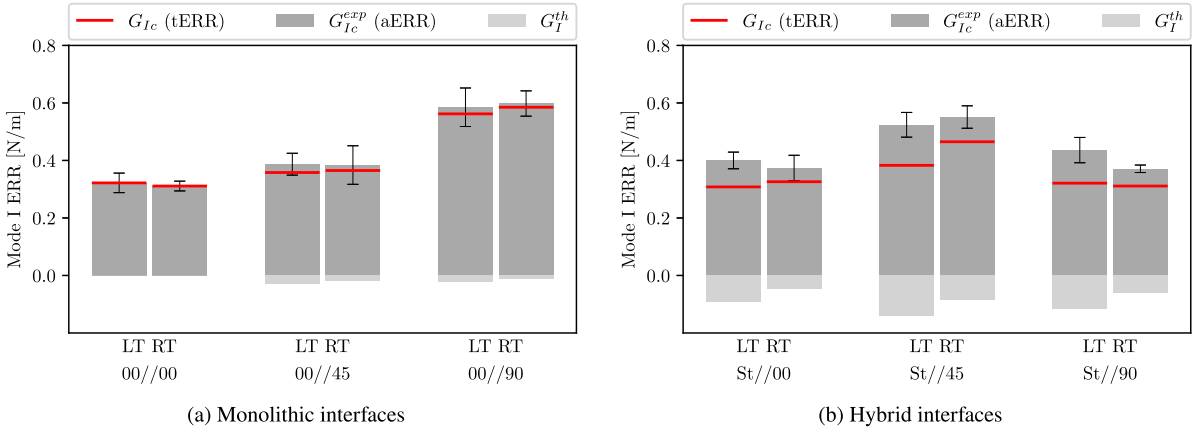

(a) Monolithic interfaces (b) Hybrid interfaces

Fig. 5. Mode I energy release rate (ERR) results for (a) monolithic and (b) hybrid interfaces including apparent ERR G_{Ic}^{exp}, thermal portion of ERR G_I^{th} and true ERR G_{Ic}.

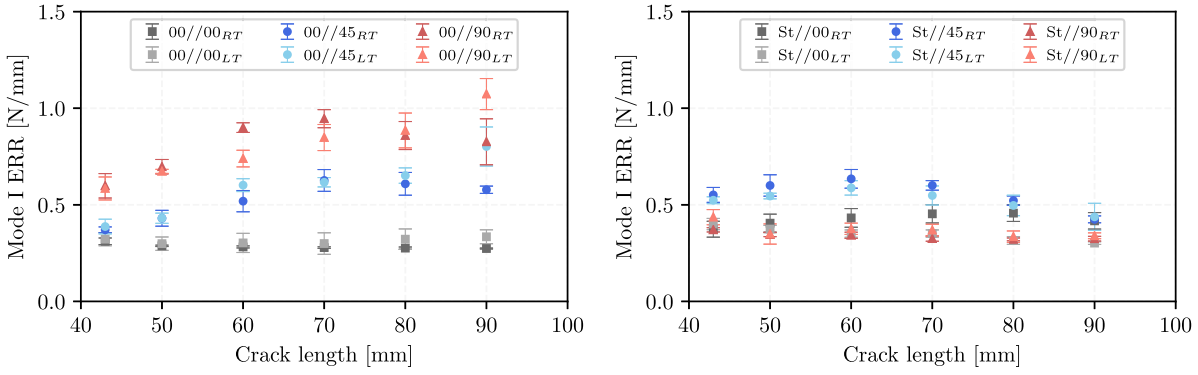

(a) Monolithic interfaces (b) Hybrid interfaces

Fig. 6. Evolution of apparent mode I energy release rate (ERR) with increasing crack length for (a) monolithic and (b) hybrid interfaces at RT and LT.

to literature results, the present observation agrees well with results by Asp [32] and contradict findings by Kim et al. [33] and Coronado et al. [36], despite similar CFRP materials and comparable stacking sequences. However, in contrast to the other studies, the present one introduces a natural pre-crack. In case of the hybrid interfaces, differences in the fracture toughness values due to temperature are rather small and mostly within the standard deviation of the experiments. Therein, the interface toughness of St//00 and St//90 appears more or less constant. However, when looking at the tERR of the interface St//45, a slight decreases with decreasing temperature is observed.

3.1.3. R-curve behavior

In order to study the R-curve behavior, the evolution of the aERR with increasing crack length is presented for both monolithic and hybrid interfaces for both RT and LT in Fig. 6.

Only the monolithic interfaces 00//45 and 00//90 exhibit a pronounced R-curve behavior. The R-curve behavior is due to the presence of fiber bridging and crack jumping during the test, see Fig. 7. This observation is in accordance with the observations made on the force–displacement curves of the DCB test. All remaining interfaces show no significant increase in fracture toughness with increasing crack length. In case of the hybrid interfaces, an R-curve behavior can only occur in case of crack jumping from the CFRP//metal interface to a CFRP//CFRP interface, thereby enabling fiber-bridging and/or the activation of multiple crack-planes at once. Both [10] reports an R-curve behavior for the St//00 interface at RT, however the present results do not confirm that observation. Here, neither the behavior of the force–displacement curve nor the evolution of ERR with increasing crack length imply R-curve behavior for the St//00 interface. This is equally the case for the St//90 interface.

Regarding the effect of temperature, it is concluded that there is no influence on the R-curve behavior for mode I delamination, as the qualitative curve shapes appear to be independant of the temperature level.

When comparing the crack paths on the specimen sides in Fig. 7, large differences between monolithic and hybrid interfaces can be seen. Fiber-bridging and crack-jumping is severely present at the 00//45 and 00//90 interfaces. Thus, the test data post crack initiation in those specimens is significantly affected by these phenomena, which also explains the R-curve behavior. However, when considering the hybrid interfaces, a crack jump right after crack initiation can be seen, but no further jumps of the crack plane during crack propagation. Thereby, indicating that the fracture toughness at crack initiation (cERR) is valid for the interfaces but values after the occurrence of the crack jump do not represent the correct delamination plane anymore.

No noticeable changes due to decreasing temperature can be seen in the shape of the crack paths for the hybrid specimens. While this is also the case for the monolithic interfaces 00//00 and 00//90, the interface 00//45 exhibits more crack-jumping with lower testing temperature. In general, the shape of the crack paths of the hybrid specimens appears smoother compared to the monolithic specimens. This is in alignment with the observations from the analysis of the force–displacement curves as well as the analysis of the R-curve behavior. Therein, the presence of fiber-bridging and crack plane jumping correlates with the presence of R-curve behavior in the monolithic specimens.

3.1.4. Fracture surfaces

Fig. 8 shows the fracture surfaces of the hybrid interfaces after testing at RT and LT. The metal surfaces, which are representative for the respective test series, are obtained manually by separation of the

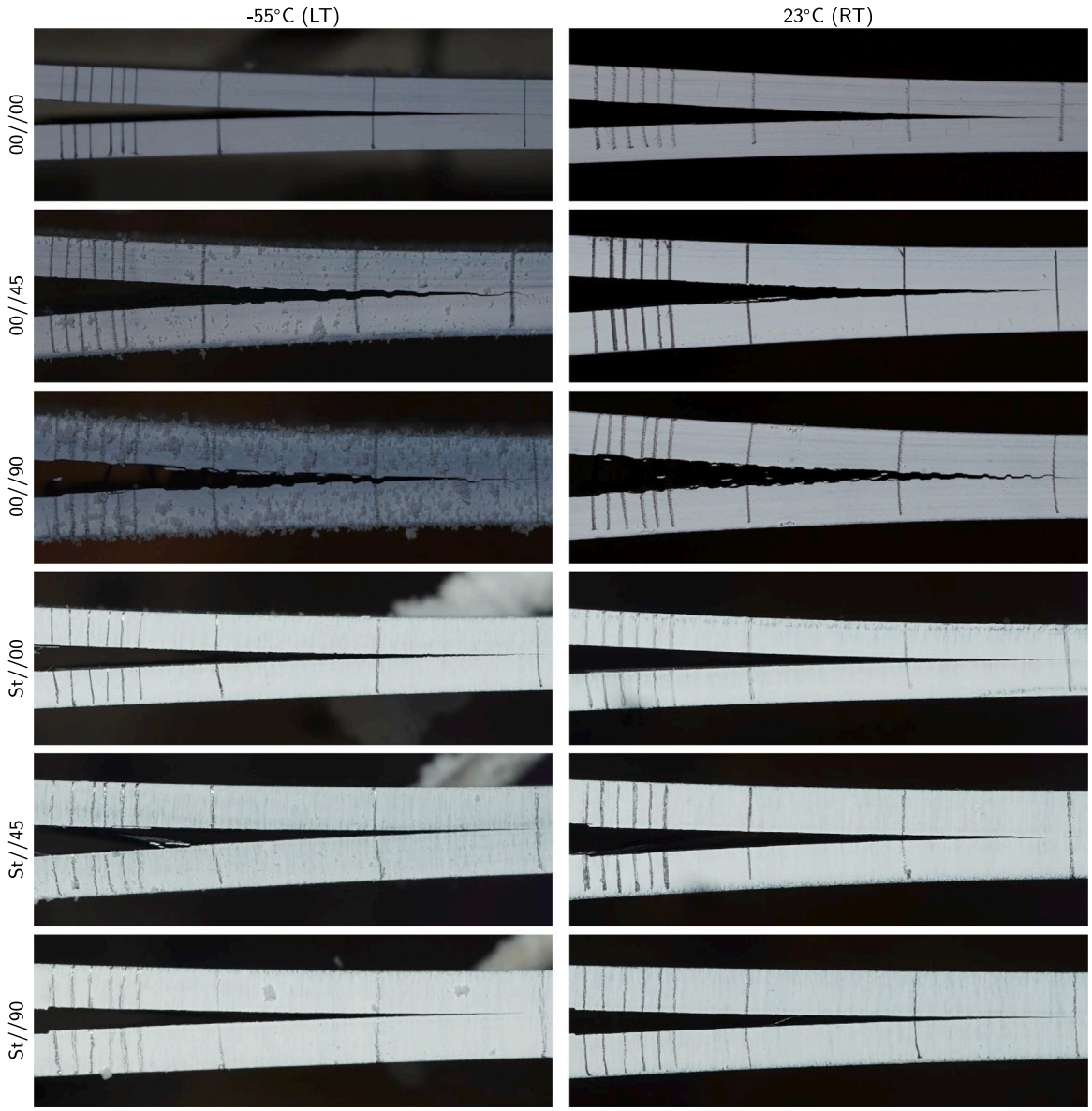

Fig. 7. Crack paths in DCB specimens at a crack length of approximately 70 mm.

sublaminates after the DCB test. Comparison of interfaces tested at LT and RT shows no qualitative differences, as expected considering the previous results regarding both ERR and force–displacement data.

Analysis of Fig. 8 reveals that the crack leaves the initial crack plane as defined by the PTFE-foil at least to some extent. For the St//45 and St//90 interfaces, the crack plane jump is facilitated through intralaminar failure. Similar behavior has been previously reported by Petersen [9] and Both [10] for FMLs and is also frequently observed in monolithic specimens [20]. The pre-crack, i.e. the initial delamination plane, is defined by the PTFE-insert, thus only the cERR at initiation of crack propagation is considered the valid fracture toughness for the respective interfaces. Values past this point are highly affected by crack-jumping. As a result, data during crack propagation is not solely representative of the initial delamination plane, thereby also explaining the large deviations in the force–displacement data especially for interfaces containing 45° and 90° layers.

3.2. Interlaminar behavior in mode II

The results of the ENF test are discussed similarly to the DCB case by first studying the force–displacement curves, then comparing cERR at delamination initiation with a focus on TRS, and eventually investigating the fracture surfaces of hybrid specimens.

3.2.1. Force–displacement curves

Fig. 9 shows the force–displacement curves of the monolithic and hybrid interfaces in the ENF test at RT and LT. For verification, analytical curves based on the equations in Appendix B are plotted using temperature-dependent material properties and tERR as input. In case of the monolithic interfaces, agreement regarding initial stiffness is excellent, while the analytically predicted crack onset slightly precedes the experimental results.

3.2.2. Critical energy release rates

In Fig. 10, the fracture toughness results from ENF testing are presented for multi-directional monolithic and hybrid interfaces at RT

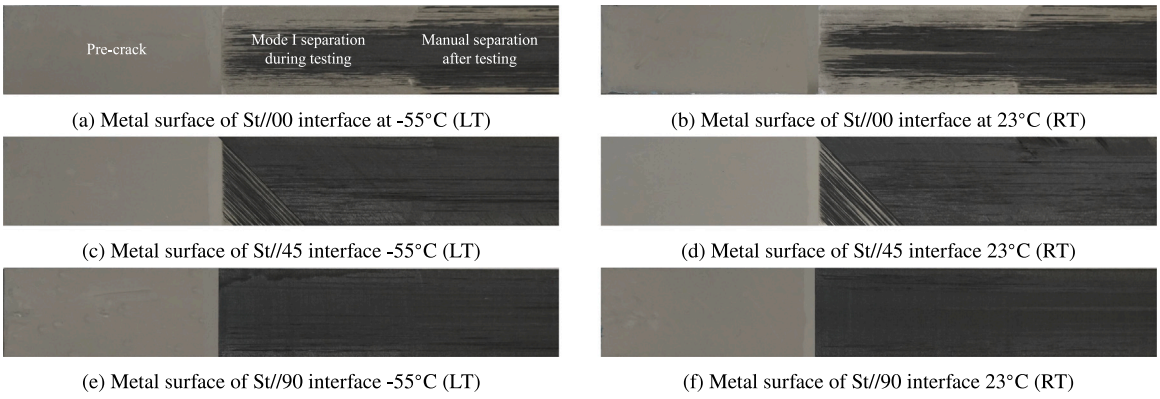

(a) Metal surface of St//00 interface at -55°C (LT)

(b) Metal surface of St//00 interface at 23°C (RT)

(c) Metal surface of St//45 interface -55°C (LT)

(d) Metal surface of St//45 interface 23°C (RT)

(e) Metal surface of St//90 interface -55°C (LT)

(f) Metal surface of St//90 interface 23°C (RT)

Fig. 8. Fracture surfaces of hybrid DCB specimens.

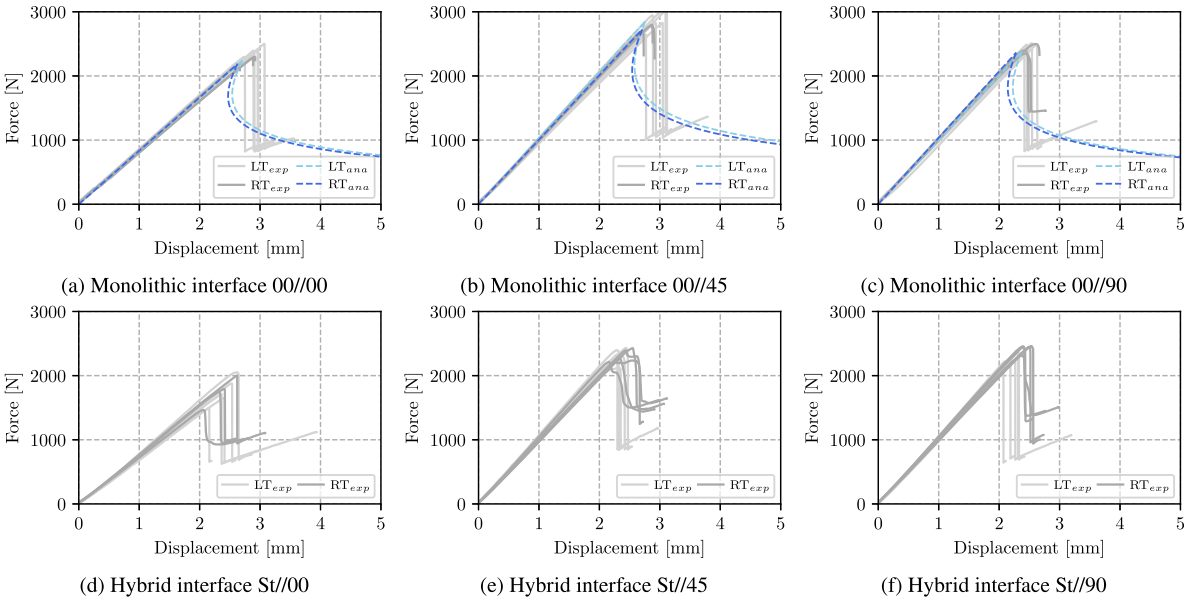

(a) Monolithic interface 00//00

(b) Monolithic interface 00//45

(c) Monolithic interface 00//90

(d) Hybrid interface St//00

(e) Hybrid interface St//45

(f) Hybrid interface St//90

Fig. 9. Force–displacement curves of ENF tests at 23 °C (RT) and −55 °C (LT).

and LT. Based on the approach to determine tERR values in Fig. 1, the aERR based on the experimental test G_{IIc}^{exp}, the thermal portion due to the asymmetric layup G_{II}^{th} as well as the tERR G_{IIc} are quantified and displayed.

As previously concluded during analysis of the DCB test results, the correction of the fracture toughness for thermal effects can be neglected for the monolithic interfaces under mode II loading, too. The correction terms are generally smaller than the standard deviation during testing, and therefore not significant. Nonetheless, in comparison with DCB case the correction terms for the monolithic interfaces in the ENF setup are considerably larger, accounting for up to 7% of the aERR in case of the 00//45 interface. In case of hybrid interfaces, inclusion of thermal effects into the data reduction process is crucial. Contrary to the DCB case where the tERR is lower than the aERR, taking into account thermal portions of the ERR results is significantly higher tERR for all interfaces in the ENF test. It should be noted that the orientation of the specimen has an influence in the ENF setup. Depending on whether the steel ply is part of the top or bottom sublaminate, the curvature of the specimen is either aligning with the loading direction or opposite to it, thus thermal effects can lead to either an increasing or decreasing contribution to the ERR. In the present case, specimens are inserted into the test rig in a way that the metal layer is always on the lower sublaminate, therefore leading to a positive contribution that is added on top of the experimentally determined ERR. A more detailed analysis of the orientation of the specimen in the ENF test and the resulting implications for the tERR is presented in Koord et al. [44].

Decreasing the testing temperature translates to a slight increase in fracture toughness in case of the interfaces 00//00 and 00//45, while the cERR of the 00//90 interface remains unaffected. The present observation is consistent with findings reported by Asp [32] for temperatures between RT and −50 °C. When decreasing the testing temperature, the interface toughness of the St//00 and St//45 interfaces increase, while the properties of the St//90 interface slightly decreases. This behavior is similar to the behavior of the monolithic interfaces under mode II loading. However, compared to the monolithic interfaces, the tERR of the hybrid interfaces exhibit lower values. It should be mentioned, however, that the differences in fracture toughness between different temperature levels are barely larger than the standard deviation during testing, and therefore should be interpreted with care. Given the fact that the fracture surfaces of the different interfaces in Fig. 11 do not exhibit noticeable differences, it is assumed that no phenomenologically different behavior occurs between RT and LT.

3.2.3. Fracture surfaces

The fracture surfaces of the hybrid ENF specimens are presented in Fig. 11. The surfaces are representative for their respective test series and are obtained by manually separating the sublaminates after testing.

The surfaces of the specimens in Fig. 11 can be divided in three areas: the area of the PTFE insert on the left (metallic blank), the area

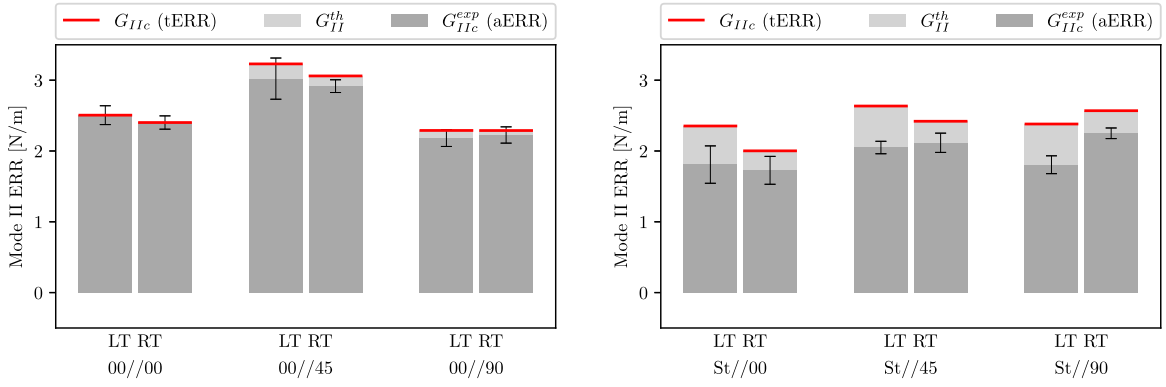

(a) Monolithic interfaces (b) Hybrid interfaces

Fig. 10. Mode II energy release rate (ERR) results for (a) monolithic and (b) hybrid interfaces including apparent ERR G_{IIc}^{exp}, thermal portion of ERR G_{II}^{th} and true ERR G_{IIc}.

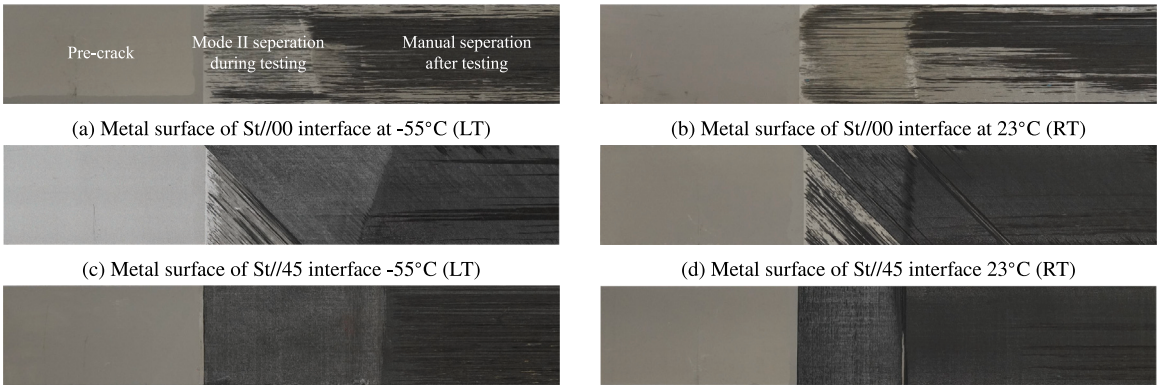

(a) Metal surface of St//00 interface at -55°C (LT)

(b) Metal surface of St//00 interface at 23°C (RT)

(c) Metal surface of St//45 interface -55°C (LT)

(d) Metal surface of St//45 interface 23°C (RT)

(e) Metal surface of St//90 interface -55°C (LT)

(f) Metal surface of St//90 interface 23°C (RT)

Fig. 11. Fracture surfaces of hybrid ENF specimens.

of mode II separation during ENF testing in the center, and the area on the right characterized by mode I separation during manual separation of the specimen halves. The hybrid interfaces tested in the ENF setup at RT and LT show no qualitative differences as already noted for the DCB specimens. The metal surface of the St//00 interface in Figs. 11(a) and 11(b) indicates that the crack remains in the initial delamination plane during crack propagation. This behavior differs from the behavior of the remaining specimens as crack-jumping is present at least partially for the St//00 interface under mode I loading and in both delamination modes for the St//45 and St//90 interfaces. Since the initial pre-crack is introduced by a PTFE-foil, determination of the mode II cERR only at crack initiation is considered valid for the respective interfaces.

4. Conclusion

In the present research, interlaminar testing by means of the DCB and ENF setups is conducted with a focus on the effects of multi-material interfaces, multi-directional interfaces and temperature.

Considering multi-directional interfaces, the fracture toughness in mode I is lowest for the 00//00 interface. Using this fracture toughness for interfaces composed of layers of different orientations can be considered conservative. However, in case of the 00//90 interface, this approach would lead to an underestimation of almost 200%. An R-curve behavior is observed for the 00//45 and 00//90 interfaces in the DCB tests due to fiber-bridging and crack-jumping. In mode II, the interlaminar fracture toughness is highest for the 00//45 interface, while the 00//00 and 00//90 exhibit lower values. Multi-directional interfaces in hybrid specimens behave very similar to monolithic interfaces. Except for the interface St//90, which exhibits significantly lower fracture toughness than its monolithic counterpart 00//90.

For multi-material interfaces, thermal correction of the aERR is considered necessary. Otherwise, no appropriate comparison between the fracture toughness of monolithic and hybrid interfaces is possible. For instance, comparing the aERR of monolithic and hybrid interfaces in mode I falsely indicates that the interface strengths of the St//00 and St//45 interfaces are significantly larger than those of their respective monolithic counterparts, 00//00 and 00//45. However, when comparing the tERR, where thermal effects are accounted for, the fracture toughness of the hybrid interfaces approach the values of the monolithic interfaces. In general, the fracture toughness of the hybrid interfaces is on the same level as is the case for monolithic interfaces, except for the St//90 interface in mode I and the St//45 interface in mode II, which exhibit noticeably lower fracture toughness compared to the 00//90 and 00//45 interfaces. Considering the crack paths in the DCB specimens, hybrid interfaces generally exhibit smooth crack path shapes, whereas the monolithic interfaces are affected by fiber bridging and crack jumping.

Decreasing testing temperatures has a limited effect on the interlaminar fracture toughness. In mode I, the tERR generally remains either almost unchanged or at least within the standard deviation of the experiment. Only in case of the St//45 interface, the fracture toughness decreases with decreasing temperature. These findings agree well with literature regarding monolithic interfaces at LT. For CFRP//steel interfaces at LT these findings are new. The crack paths at low temperature appear slightly sharper and more brittle in monolithic interfaces, while no noticeable difference is observed on the crack paths of hybrid specimens. In mode II, the fracture toughness of monolithic interfaces again appear unaffected by the change in temperature. In case of the hybrid specimens, the interface toughness increases for St//00 and

St//45, but decreases for St//90. However, it should be mentioned that the differences are barely larger than the standard deviation during testing.

CRediT authorship contribution statement

J. Koord: Writing – review & editing, Writing – original draft, Visualization, Validation, Software, Project administration, Methodology, Investigation, Formal analysis, Data curation, Conceptualization. **C. Hühne:** Supervision, Resources, Project administration, Funding acquisition.

Declaration of competing interest

The authors declare that they have no known competing financial interests or personal relationships that could have appeared to influence the work reported in this paper.

Data availability

The data is part of ongoing research.

Appendix A. Analytical formulation DCB test

For verification of the experimental results, the analytical formulation of the force–displacement behavior from Harper and Hallett [59] are applied. As the formulation is derived for a symmetric DCB specimen with identical half-beams, the application to multi-directional and multi-material interfaces is limited. For small asymmetry effects, however, the formulation is deemed sufficiently accurate. The tip opening displacement δ_I and mode I ERR G_I are described using the cantilever longitudinal stiffness E_x, the second moment of inertia of a cantilever arm I and the thickness of a cantilever arm h:

$$\delta_I = \frac{2P(a+\chi h)^3}{3E_x I} \tag{6}$$

$$G_I = \frac{P^2(a+\chi h)^3}{bE_x I} \tag{7}$$

With the correction parameter χ, the simple beam theory is extended to account for shear deformation and for local deformations at the crack tip:

$$\chi = \sqrt{\frac{E_x}{11G_{xz}}\left[3 - 2\left(\frac{\Gamma}{1+\Gamma}\right)^2\right]} \tag{8}$$

$$\Gamma = 1.18\frac{\sqrt{E_x E_y}}{G_{xz}} \tag{9}$$

In the elastic regime, i.e. before crack propagation, the resulting force P and ERR G_I are the result of an incrementally increasing tip displacement δ_I. Once the condition $G_I = G_{Ic}$ is met, the subsequent regime of stable crack propagation can be calculated using the same equations with G_I set to G_{Ic} (i.e. tERR).

Appendix B. Analytical formulation ENF test

Harper and Hallett [59] also provide an analytical formulation for the force–displacement curves of the ENF test. The center stamp displacement δ_{II} and mode II ERR G_{II} are calculated as follows:

$$\delta_{II} = \frac{3P(a+0.42\chi h)^3 + 2P(L/2)^3}{96E_x I} \tag{10}$$

$$G_{II} = \frac{3P^2(a+0.42\chi h)^2}{64bE_x I} \tag{11}$$

In addition to the specimen geometry and correction factors that can be adopted from the DCB setup, the distance between the supporting leg and load stamp $L/2$ is introduced. The force–displacement curve is determined analogous to the DCB case.

Appendix C. Correction of thermal effects

In the following, the definitions of the variables in Eqs. (4) and (5) are presented. Appendix C.1 shows the method for correcting the fracture toughness for the effect of TRS excluding tip forces, while Appendix C.2 provides the correction term for the fracture toughness due to tip forces.

C.1. Thermal portion of ERR in bonded and unbonded area

Derivation of the variables of the correction method is based on CLT. A detailed derivation of the method is presented in Yokozeki et al. [45].

$$\begin{bmatrix} N^{(k)} \\ M^{(k)} \end{bmatrix} = \begin{bmatrix} A_{11}^{(k)} & B_{11}^{(k)} \\ B_{11}^{(k)} & D_{11}^{(k)} \end{bmatrix} \begin{bmatrix} \varepsilon_0^{(k)} \\ \kappa^{(k)} \end{bmatrix} - \begin{bmatrix} N_T^{(k)} \\ M_T^{(k)} \end{bmatrix} \Delta T \tag{12}$$

$$\begin{aligned} A_{11}^{(k)} &= b\sum_i E_i^{(k)}(z_i^{(k)} - z_{i-1}^{(k)}), \\ B_{11}^{(k)} &= \frac{1}{2}b\sum_i E_i^{(k)}(z_i^{(k)2} - z_{i-1}^{(k)2}), \\ D_{11}^{(k)} &= \frac{1}{3}b\sum_i E_i^{(k)}(z_i^{(k)3} - z_{i-1}^{(k)3}), \\ N_T^{(k)} &= b\sum_i E_i^{(k)}\alpha_i^{(k)}(z_i^{(k)} - z_{i-1}^{(k)}), \\ M_T^{(k)} &= b\frac{1}{2}\sum_i E_i^{(k)}\alpha_i^{(k)}(z_i^{(k)2} - z_{i-1}^{(k)2}), \end{aligned} \tag{13}$$

$$\begin{aligned} C_k^{(k)} &= \frac{A_{11}^{(k)}}{A_{11}^{(k)}D_{11}^{(k)} - B_{11}^{(k)2}}, \qquad C_\varepsilon^{(k)} = \frac{D_{11}^{(k)}}{A_{11}^{(k)}D_{11}^{(k)} - B_{11}^{(k)2}}, \\ D^{(k)} &= \frac{-B_{11}^{(k)}}{A_{11}^{(k)}D_{11}^{(k)} - B_{11}^{(k)2}}, \\ \alpha_\varepsilon^{(k)} &= \frac{D_{11}^{(k)}N_T^{(k)} - B_{11}^{(k)}M_T^{(k)}}{A_{11}^{(k)}D_{11}^{(k)} - B_{11}^{(k)2}}, \qquad \alpha_k^{(k)} = \frac{A_{11}^{(k)}M_T^{(k)} - B_{11}^{(k)}N_T^{(k)}}{A_{11}^{(k)}D_{11}^{(k)} - B_{11}^{(k)2}} \end{aligned} \tag{14}$$

$$I^{(k)} = N_T^{(k)}\alpha_\varepsilon^{(k)} + M_T^{(k)}\alpha^{(k)2} - b\sum_i E_i^{(k)}\alpha_i^{(k)}t_i^{(k)} \tag{15}$$

C.2. Thermal portion of ERR due to contact force at specimen end

Equations for the correction for tip forces from [55].

$$\begin{aligned} G_{I,tip}^{th} = &-\frac{EI + E_a I_a}{2\rho^2 B}\left[1 + 4\frac{EI + E_a I_a}{(h+t)^2 B}\left(\frac{1}{Et} + \frac{1}{E_a h}\right)\right] \\ &+ \frac{(\Delta\alpha\Delta T)^2}{1/E_a h + 1/Et} - \frac{3E}{8\rho^2 B}\frac{II_c}{I + I_c} \end{aligned} \tag{16}$$

$$I = \frac{Bt^3}{12} \qquad I_a = \frac{Bh^3}{12} \qquad I_c = \frac{B(t+h)^3}{12} \tag{17}$$

$$\frac{1}{\rho} = \frac{6\Delta\alpha\Delta T(1+m)^2}{(h+t)(3(1+m)^2 + (1+mn)(m^2 + 1/mn))} \tag{18}$$

$m = h/t$ and $n = E_a/E$

References

[1] Holleman E. GLARE development - an overview. Tech. Rep. BE2040, Delft University of Technology; 1994.

[2] Beumler T. Flying GLARE a contribution to aircraft certification issues in strength properties in non-damaged and fatigue damaged GLARE structures. Delft: Delft University Press; 2004.

[3] Hagenbeek M. Characterisation of fibre metal laminates under thermomechanical loadings. (Ph.D. thesis), TU Delft; 2005.

[4] Miller JL, Progar DJ, Johnson WS, St. Clair TSL. Preliminary evaluation of hybrid titanium composite laminates. J Adhes 1995;54(1–4):223–40. http://dx.doi.org/10.1080/00218469508014392.

[5] Le Bourlegat LR, Damato CA, da Silva DF, Botelho EC, Pardini LC. Processing and mechanical characterization of titanium-graphite hybrid laminates. J Reinf Plast Compos 2010;29(22):3392–400, doi:10.1177/0731684410377541.

[6] Silva DF, Botelho EC, Ancelotti AC, Damato CA. Environmental conditioning effects on the mechanical properties of titanium fiber-metal-laminates.

[7] Hundley JM, Hahn HT, Yang J-M, Facciano AB. Three-dimensional progressive failure analysis of bolted titanium-graphite fiber metal laminate joints. J Compos Mater 2011;45(7):751–69, doi:10.1177/0021998310391047.

[8] Fink A, Camanho PP, Andr'es JM, Pfeiffer E, Obst A. Hybrid cfrptitanium bolted joints performance assessment and application to a spacecraft payload adaptor. Compos Sci Technol 2010;70(2):305–17, https://doi.org/10.1016/j.compscitech.2009.11.002.

[9] Petersen E. Untersuchung des metalllagenauslaufs bei lokaler stahlhybridisierung von kohlenstofffaserkunststofflaminaten unter berücksichtigung des phänomenologischen strukturverhaltens. (Ph.D. thesis), TU Braunschweig; 2019.

[10] Both JC. TragfÄhigkeit von cfk-metall-laminaten and unter and mechanischer und thermischer belastung. (Ph.D. thesis), Technische Universität München; 2013, URL https://mediatum.ub.tum.de/doc/1173300/1173300.pdf.

[11] Boose Y, Kappel E, Stefaniak D, Prussak R, Pototzky A, Weiß L. Phenomenological investigation on crash characteristics of thin layered cfrp-steel laminates. Int J Crashworthiness 2022;27(1):289–98, doi:10.1080/13588265.2020.1787681.

[12] Ramulu M, Branson T, Kim D. A study on the drilling of composite and titanium stacks. Compos Struct 2001;54(1):67–77, https://doi.org/10.1016/S0263-8223(01)00071-X.

[13] Stefaniak D. Improving the mechanical performance of unidirectional CFRP by metal-hybridization. In: ECCM15-15th European conference on composite materials. Padova: Juni, Venedig; 2012, p. 24–8.

[14] Prussak R, Stefaniak D, Huhne C, Sinapius M. Evaluation of residual stress development in FRP-metal hybrids using fiber bragg grating sensors. Prod Eng 2018;12(2):259–67, doi:10.1007/s11740-018-0793-4.

[15] Petersen E, Stefaniak D, Huhne C. Experimental investigation of load carrying mechanisms and failure phenomena in the transition zone of locally metal reinforced joining areas. Compos Struct 2017;182:79–90, doi:10.1016/j.compstruct.2017.09.002.

[16] Petersen E, Koord J, Völkerink O, Stefaniak D, Hühne C. Experimental and numerical investigation of the transition zone of locally steel-reinforced joining areas under combined tension–bending loading. J Compos Mater 2020;54(17):2339–52, doi:10.1177/0021998319893729.

[17] Monden A. Adhäsion zwischen epoxidharzbasiertem cfk und oberflächenmodifiziertem stahl: grenzschichtversagen von hybridlaminaten unter mode i, mode ii und mixed-mode belastung. (Ph.D. thesis), Universität Augsburg; 2016, http://dx.doi.org/10.13140/rg.2.2.11923.89120.

[18] ASTM D5528-13. Test method for mode i interlaminar fracture toughness of unidirectional fiber-reinforced polymer matrix composites. 2013, http://dx.doi.org/10.1520/D5528-13.

[19] ASTM D7905-19. Test method for determination of the mode II interlaminar fracture toughness of unidirectional fiber-reinforced polymer matrix composites. 2019, http://dx.doi.org/10.1520/D7905_D7905M-19E01.

[20] Pereira A, de Morais A. Mode i interlaminar fracture of carbon/epoxy multidirectional laminates. Compos Sci Technol 2004;64(13–14):2261–70. http://dx.doi.org/10.1016/j.compscitech.2004.03.001.

[21] Pereira AB, Morais ABd, Marques AT, Castro PTd. Mode II interlaminar fracture of carbonepoxy multidirectional laminates. Compos Sci Technol 2004;64(10–11):1653–9, doi:10.1016j.compscitech.2003.12.001.

[22] Morais Ad, Moura Md, Gonccalves J, Camanho P. Analysis of crack propagation in double cantilever beam tests of multidirectional laminates. Mech Mater 2003;35(7):641–52, doi:10.1016S0167-6636(02)00289-2.

[23] Völkerink O, Koord J, Petersen E, Hühne C. Holistic determination of physical fracture toughness values and numerical parameters for delamination analysis considering multidirectional-interfaces. Compos Part C: Open Access 2022;8:100277. http://dx.doi.org/10.1016/j.jcomc.2022.100277.

[24] Greenhalgh ES. Failure analysis and fractography of polymer composites. Cambridge: Woodhead Publishing in materials, Woodhead Pub.; 2009.

[25] Park J-S, Kim J-H, Park J-H, Ko D-C. Prediction of the delamination at the steel and CFRP interface of hybrid composite part. Materials 2021;14(21):6285. http://dx.doi.org/10.3390/ma14216285.

[26] Yao Y, Shi P, Chen M, Chen G, Gao C, Boisse P, Zhu Y. Experimental and numerical study on mode i and mode II interfacial fracture toughness of co-cured steel-CFRP hybrid composites. Int J Adhes Adhes 2022;112:103030. http://dx.doi.org/10.1016/j.ijadhadh.2021.103030.

[27] Sinmazçelik T, Avcu E, Özgür Bora M, Çoban O. A review: Fibre metal laminates, background, bonding types and applied test methods. Mater Des 2011;32(7):3671–85. http://dx.doi.org/10.1016/j.matdes.2011.03.011.

[28] Petersen E, Kappel E, Koord J, Völkerink O, Hühne C. Determination of stresses, strains and failure types in multidirectional laminates under pure bending. J Compos Mater 2020;54(28):4397–413. http://dx.doi.org/10.1177/0021998320932301.

[29] Chai H. Interlaminar shear fracture of laminated composites. Int J Fract 1990;43(2):117–31. http://dx.doi.org/10.1007/bf00036181.

[30] Tao J, Sun CT. Influence of ply orientation on delamination in composite laminates. J Compos Mater 1998;32(21):1933–47. http://dx.doi.org/10.1177/002199839803202103.

[31] Bieniaś J, Dadej K, Surowska B. Interlaminar fracture toughness of glass and carbon reinforced multidirectional fiber metal laminates. Eng Fract Mech 2017;175:127–45. http://dx.doi.org/10.1016/j.engfracmech.2017.02.007.

[32] Asp L. The effects of moisture and temperature on the interlaminar delamination toughness of a carbon/epoxy composite. Compos Sci Technol 1998;58(6):967–77. http://dx.doi.org/10.1016/s0266-3538(97)00222-4.

[33] Kim HS, Wang W-X, Takao Y. Effects of temperature and fiberorientation on the mode i interlaminar fracture toughness of carbon/epoxy composites. In: ICCM12. 1999.

[34] Coronado P, Argüelles A, Viña J, Mollón V, Viña I. Influence of temperature on a carbon–fibre epoxy composite subjected to static and fatigue loading under mode-i delamination. Int J Solids Struct 2012;49(21):2934–40. http://dx.doi.org/10.1016/j.ijsolstr.2012.05.018.

[35] Coronado P, Argüelles A, Viña J, Viña I. Influence of low temperatures on the phenomenon of delamination of mode i fracture in carbon-fibre/epoxy composites under fatigue loading. Compos Struct 2014;112:188–93. http://dx.doi.org/10.1016/j.compstruct.2014.02.007.

[36] Coronado P, Camanho P, Argüelles A, Viña J, Sánchez S. Low temperature and resin effects on the mode i interlaminar fracture toughness in aeronautical quality polymer composites. Proceedings 2018;2(23):1478. http://dx.doi.org/10.3390/proceedings2231478.

[37] Alderliesten R. Fatigue and fracture of fibre metal laminates. Springer International Publishing; 2017, http://dx.doi.org/10.1007/978-3-319-56227-8.

[38] Rans C, Alderliesten R. The influence of temperature on crack growth in fibre metal laminates. In: 12th international conference on fracture. 2009.

[39] Schut AR, JE. Delamination growth rate at low and elevated temperatures in glare. In: 25TH international congress of the aeronautical sciences (ICAS 2006). 2006.

[40] Burianek DA, Spearing S. Delamination growth from face sheet seams in cross-ply titanium/graphite hybrid laminates. Compos Sci Technol 2001;61(2):261–9. http://dx.doi.org/10.1016/s0266-3538(00)00206-2.

[41] Rans C, Alderliesten R, Benedictus R. Predicting the influence of temperature on fatigue crack propagation in fibre metal laminates. Eng Fract Mech 2011;78(10):2193–201. http://dx.doi.org/10.1016/j.engfracmech.2011.04.005.

[42] Nairn JA. On the calculation of energy release rates for cracked laminates with residual stresses. Int J Fract 2006;139(2):267–93. http://dx.doi.org/10.1007/s10704-006-0044-0.

[43] Wang W, Freitas STD, Poulis JA, Zarouchas D. A review of experimental and theoretical fracture characterization of bi-material bonded joints. Composites B 2021;206:108537. http://dx.doi.org/10.1016/j.compositesb.2020.108537.

[44] Koord J, Völkerink O, Petersen E, Hühne C. Effect of low temperature on mode i and mode II interlaminar fracture toughness of CFRP-steel hybrid laminates. Composites B 2023;262:110773. http://dx.doi.org/10.1016/j.compositesb.2023.110773.

[45] Yokozeki T, Ogasawara T, Aoki T. Correction method for evaluation of interfacial fracture toughness of DCB, ENF and MMB specimens with residual thermal stresses. Compos Sci Technol 2008;68(3–4):760–7. http://dx.doi.org/10.1016/j.compscitech.2007.08.025.

[46] ASTM D6671-19. Standard test method for mixed mode i-mode ii interlaminar fracture toughness of unidirectional fiber reinforced polymer matrix composites. 2019, http://dx.doi.org/10.1520/D6671_D6671M-19.

[47] Connolly JV. Application of fracture mechanics to composite materials. amsterdam: elsevier science publishers; 1989, p. 671. http://dx.doi.org/10.1017/S0001924000023137, The Aeronautical Journal (1968) 94 (938) (1990) 295–295,

[48] Choi NS, Kinloch AJ, Williams JG. Delamination fracture of multidirectional carbon-fiber/epoxy composites under mode i, mode ii and mixed-mode i/ii loading. J Compos Mater 1999;33(1):73–100. http://dx.doi.org/10.1177/002199839903300105.

[49] Robinson P, Song D. A modified dcb specimen for mode i testing of multidirectional laminates. J Compos Mater 1992;26(11):1554–77. http://dx.doi.org/10.1177/002199839202601101.

[50] Stefaniak D. Improving residual strength of unidirectionally reinforced plastic laminates by metal layering. (Ph.D. thesis), TU Braunschweig; 2017.

[51] Prombut P, Michel L, Lachaud F, Barrau J. Delamination of multidirectional composite laminates at $0°/\theta°$ ply interfaces. Eng Fract Mech 2006;73(16):2427–42. http://dx.doi.org/10.1016/j.engfracmech.2006.05.013.

[52] Koord J, Stüven J-L, Petersen E, Völkerink O, Hühne C. Investigation of exact analytical solutions for circular notched composite laminates under tensile loading. Compos Struct 2020;243:112180. http://dx.doi.org/10.1016/j.compstruct.2020.112180.

[53] Koord J, Stüven J-L, Völkerink O, Petersen E, Hühne C. Investigation of exact analytical solutions for composite laminates under pin-bearing loading. Compos Struct 2022;292:115605. http://dx.doi.org/10.1016/j.compstruct.2022.115605.

[54] Perez PG, Bouvet C, Chettah A, Dau F, Ballere L, Pérès P. Effect of unstable crack growth on mode II interlaminar fracture toughness of a thermoplastic PEEK composite. Eng Fract Mech 2019;205:486–97. http://dx.doi.org/10.1016/j.engfracmech.2018.11.022.

[55] Guo S, Dillard DA, Nairn JA. Effect of residual stress on the energy release rate of wedge and dcb test specimens. Int J Adhes Adhes 2006;26(4):285–94. http://dx.doi.org/10.1016/j.ijadhadh.2005.04.002, URL https://www.sciencedirect.com/science/article/pii/S0143749605000680.

[56] Pagano NJ, Hahn HT. Evaluation of composite curing stresses, in: solid mechanics and its applications. Netherlands: Springer; 1994, p. 57–69. http://dx.doi.org/10.1007/978-94-017-2233-9_6.

[57] Tsokanas P, Loutas T, Pegkos D, Sotiriadis G, Kostopoulos V. Mode II fracture toughness of asymmetric metal-composite adhesive joints. MATEC Web Conf 2019;304:01004. http://dx.doi.org/10.1051/matecconf/201930401004.

[58] Loutas T, Tsokanas P, Kostopoulos V, Nijhuis P, van den Brink WM. Mode i fracture toughness of asymmetric metal-composite adhesive joints. Mater Today: Proc 2020. http://dx.doi.org/10.1016/j.matpr.2020.03.075.

[59] Harper PW, Hallett SR. Cohesive zone length in numerical simulations of composite delamination. Eng Fract Mech 2008;75(16):4774–92. http://dx.doi.org/10.1016/j.engfracmech.2008.06.004.